Variation of band bending at the surface of Mg-doped InGaN: Evidence of *p*-type conductivity across the composition range

P. D. C. King, T. D. Veal, P. H. Jefferson, and C. F. McConville*
Department of Physics, University of Warwick, Coventry CV4 7AL, United Kingdom

Hai Lu† and W. J. Schaff
Department of Electrical and Computer Engineering, Cornell University, Ithaca, New York 14853, USA
(Received 12 December 2006; revised manuscript received 12 January 2007; published 12 March 2007)

The variation of band bending as a function of composition at oxidized (0001) surfaces of Mg-doped $In_xGa_{1-x}N$ is investigated using x-ray photoelectron spectroscopy. Distinctly different trends in barrier height are seen for the Mg-doped compared to undoped alloys, which is explained in terms of Fermi-level pinning at the surface and virtual gap states. Solutions of Poisson's equation within the modified Thomas-Fermi approximation are used to model the band bending and corresponding variation of carrier concentration with depth below the surface. A transition from a surface inversion layer for In-rich alloys to a surface hole depletion layer for Ga-rich alloys occurs at $x \approx 0.49$. The trend in barrier height, calculated space-charge profiles, and difference of barrier height for undoped and Mg-doped InN indicate that Mg doping induces bulk *p*-type conductivity across the entire composition range.

DOI: 10.1103/PhysRevB.75.115312 PACS number(s): 73.61.Ey, 71.55.Eq, 79.60.−i, 71.20.Nr

I. INTRODUCTION

InN and related alloys have received considerable research interest in recent years,[1,2] largely due to their potential use in device applications. The revision of the band gap to the now almost universally accepted value of approximately 0.7 eV (Refs. 3 and 4) introduced the possibility to use the InGaN ternary system in optoelectronic components spanning virtually the entire solar range. It has also been shown[5] that (especially In-rich) InGaN alloys show a higher degree of resistance to radiation damage than photovoltaic materials in common use today, suggesting their potential for use in solar cells for space applications. The surface electronic properties of the material are of crucial importance for device applications, and the transition from extreme electron accumulation (downward band bending) at the surface of *n*-type InN (Ref. 6) to electron depletion (upward band bending) at the surface of *n*-type GaN (Ref. 7) has been reported previously.[8] Due to the low Γ-point conduction-band minimum (CBM) with respect to the branch-point energy (or charge-neutrality level) in In-rich InGaN, *p*-type doping of these materials has proved extremely difficult, with success only reported recently.[9] Furthermore, an inversion layer is expected to form at *p*-type InN surfaces,[10] resulting in a layer of electrons close to the surface; consequently, measurements to demonstrate that the Mg dopants act to induce *p*-type bulk conductivity can only be achieved indirectly[9] or through methods involving complicated fitting procedures, such as quantitative mobility spectrum analysis of variable magnetic field Hall-effect data.[11] Due to these difficulties, the surface space-charge region of *p*-type InN and In-rich InGaN has not been well characterized. In contrast to InN, a hole depletion layer is reported for *p*-type GaN,[7] and the transition between these two regimes warrants further investigation.

Here, we report the variation of the surface band bending as a function of composition for Mg-doped $In_xGa_{1-x}N$ alloys as determined by high-resolution x-ray photoelectron spectroscopy (XPS) measurements of the valence band to surface Fermi-level separation. A transition from a surface inversion layer for In-rich alloys to a surface hole depletion layer for Ga-rich alloys is shown to occur at $x \approx 0.49$. This is discussed in terms of Fermi-level pinning at the surface and the existence of virtual gap states. The results are presented as evidence for *p*-type bulk conductivity across the entire composition range.

II. EXPERIMENTAL DETAILS

The Mg-doped InGaN samples were all grown on *c*-plane sapphire substrates by plasma assisted molecular-beam epitaxy using either a 200 nm thick AlN or GaN buffer layer. Details of the growth are reported elsewhere.[12] The InGaN layer thicknesses ranged from 200 to 1000 nm and growth temperatures from 530 to 740 °C measured by a thermocouple situated close to the sample, which therefore slightly overestimates the actual growth temperature. The In/Ga ratio was determined by x-ray diffraction. The Mg cell temperature was approximately 350 °C for all sample growths.

The XPS measurements were performed using a Scienta ESCA300 spectrometer at the National Centre for Electron Spectroscopy and Surface Analysis, Daresbury Laboratory, UK. X rays, of energy $h\nu = 1486.6$ eV, were produced using a monochromated rotating anode Al $K\alpha$ x-ray source. The ejected photoelectrons were analyzed by a 300 mm mean radius spherical-sector electron energy analyzer with 0.8 mm slits at a pass energy of 150 eV. The effective instrumental resolution is 0.45 eV, derived from the Gaussian convolution of the analyzer broadening and the natural linewidth of the x-ray source (0.27 eV). The binding energy scale is given with respect to the Fermi level and was calibrated using the Fermi edge of an ion-bombarded silver reference sample that is regularly used to calibrate the spectrometer. The position of the valence-band maximum (VBM) with respect to the Fermi level is determined by extrapolating a linear fit to the

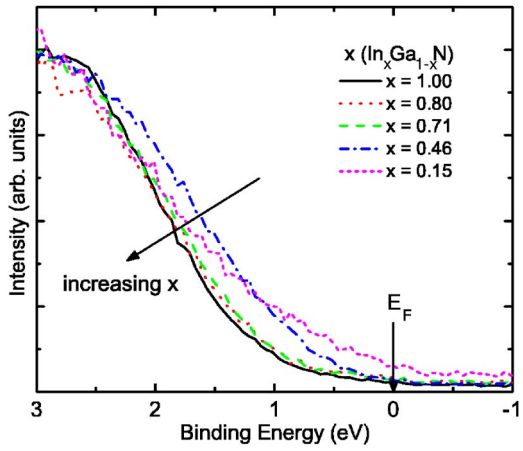

FIG. 1. (Color online) The valence-band XPS spectra for $In_xGa_{1-x}N$ alloys with respect to the Fermi level E_F. The VBM to Fermi-level separation (ξ), calculated by extrapolating a linear fit to the leading edge of the valence-band photoemission to the background level, increases (i.e., the VB edge shifts to higher binding energies) with increasing In content from $\xi=0.72\pm0.10$ eV for $In_{0.15}Ga_{0.85}N$ to $\xi=1.12\pm0.10$ eV for InN.

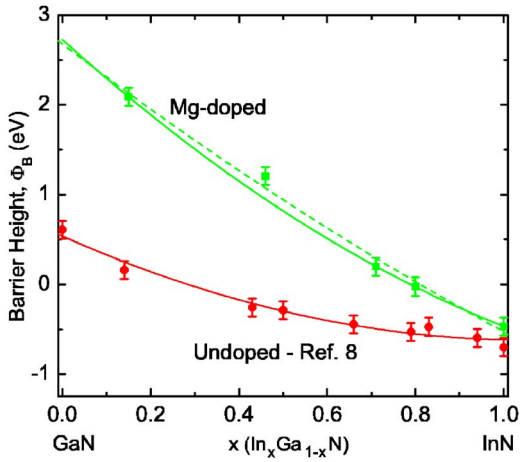

FIG. 2. (Color online) The variation of the barrier height (CBM to Fermi-level separation, Φ_B) for Mg-doped and undoped (Ref. 8) $In_xGa_{1-x}N$ alloys as a function of composition. A second-order polynomial least-squares fit to the barrier height is shown in each case. For the Mg-doped alloys, the fit is shown including (dashed line) and excluding (solid line) the $x=0.46$ value due to the lower quality of this sample compared to the In-rich and Ga-rich samples. A clear difference in barrier height is seen between the two different cases across the composition range supporting the association of the Mg-doped materials with *p*-type bulk characteristics.

leading edge of the valence-band photoemission to the background level in order to take account of the finite resolution of the spectrometer.[8,13]

Measurements are presented for as-loaded (oxidized) samples due to the difficulty in cleaning the samples without causing electronic damage.[14,15] Investigation of the In 3*d*, Ga 2*p*, N 1*s*, C 1*s*, and O 1*s* core-level peaks from XPS indicated a III-O oxide component but no significant N-O bonding. Additionally, adventitious hydrocarbons were identified on the surface.

III. RESULTS

The valence-band XPS spectra for the Mg-doped $In_xGa_{1-x}N$ samples, with respect to the Fermi level E_F, are shown in Fig. 1. In general, the VBM to Fermi-level separation (ξ) can be seen to increase with increasing In content from $\xi=0.72\pm0.10$ eV for $In_{0.15}Ga_{0.85}N$ (the most Ga-rich sample measured) to $\xi=1.12\pm0.10$ eV for InN. Incorporating the change in band gap as a function of composition, described by a bowing parameter of 1.4 eV,[16] allows a barrier height Φ_B (the CBM to Fermi-level separation, analogous to the Schottky barrier height of a semiconductor-metal junction) to be calculated. This is shown, with the equivalent values for undoped InGaN samples,[8] in Fig. 2. The measured values of the VBM to Fermi-level separation, the band-gap values used, and the resulting barrier heights for the Mg-doped $In_xGa_{1-x}N$ samples are additionally tabulated in Table I.

The Mg-doped alloys exhibit higher values of Φ_B compared to the undoped alloys across the composition range, with the largest differences for Ga-rich alloys. Second-order least-squares polynomial fits to the measured data are also shown. $In_xGa_{1-x}N$ samples are known both experimentally[17,18] and theoretically[19] to exhibit phase separation at $x\sim0.5$. Although the samples were grown under conditions to minimize phase separation,[20] the sample quality is still expected to be lower for the 46% In composition than the other more In-rich or Ga-rich samples measured. The barrier height as a function of composition for the Mg-doped alloys is therefore estimated as $\Phi_B=2.68-3.73x+0.53x^2$ and $\Phi_B=2.73-4.43x+1.24x^2$ including and excluding the $x=0.46$ sample, respectively. Better agreement with the measured In-rich and Ga-rich samples is achieved when the $x=0.46$ sample is neglected.

IV. ANALYSIS

These relations can be used to determine the surface Fermi level as a function of composition referenced to the universal branch-point energy shown in Fig. 3. If the Mg-doped samples are *p*-type in the bulk such that the bulk Fermi level lies close to the VBM, the Fermi level at the surface (which is well into the band gap or even above the

TABLE I. The valence band to Fermi-level separation, ξ, measured by x-ray photoelectron spectroscopy, the band gap E_g, and the resulting barrier height, $\Phi_B=E_g-\xi$, as a function of Mg-doped $In_xGa_{1-x}N$ alloy composition.

x	ξ (eV)	E_g (eV)	Φ_B (eV)
1.00	1.12	0.65	−0.47
0.80	1.00	0.98	−0.02
0.71	0.96	1.16	0.20
0.46	0.58	1.79	1.21
0.15	0.72	2.81	2.09

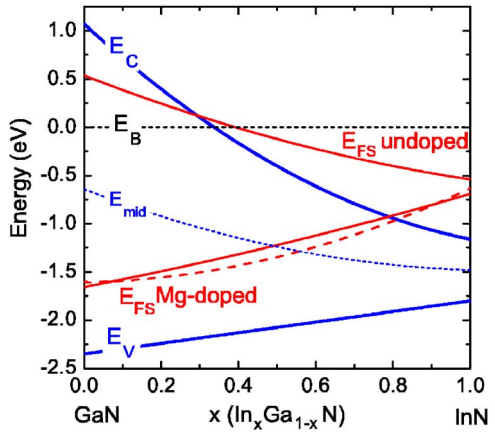

FIG. 3. (Color online) The CBM (E_C), VBM (E_V), and midgap position (E_{mid}) with respect to the universal branch point energy (E_B) as a function of $In_xGa_{1-x}N$ alloy composition. The position of E_B above the VBM [which is known to vary linearly with composition (Ref. 21)] is fixed at the GaN and InN end points at 2.35 and 1.8 eV, respectively, after Veal *et al.* (Ref. 8) based on the zero-charge-transfer Schottky barrier height (Refs. 22 and 23) and theoretical calculations (Ref. 21) for GaN and the degree of electron accumulation (Ref. 6), particle irradiation studies (Ref. 24) and theoretical calculations (Ref. 25), for InN. The bowing in the conduction-band edge is calculated assuming a band-gap bowing parameter of 1.4 eV (Ref. 16). The position of the Fermi level at the surface (E_{FS}) as determined from the photoemission results is shown for both undoped (Ref. 8) and Mg-doped materials calculated from the polynomial fit to the barrier height including (dashed line) and excluding (solid line) the $x=0.46$ sample for the Mg-doped case shown in Fig. 2. The pinning of the surface Fermi level for the Mg-doped and undoped materials is seen to diverge with increasing Ga content.

CBM) is pinned above its bulk value across the composition range. This implies a downward bending of the CBM and VBM with respect to the Fermi level at the surface across the composition range resulting in a space-charge region, although the exact degree of band bending, and hence type of space-charge region, is dependent on the relative positions of the surface and bulk Fermi levels of a specific sample.

It is informative to consider specific examples of the band bending and carrier-concentration profiles. The spatial dependence of the band bending in the space-charge region is described by a potential, $V(z)$, which must satisfy Poisson's equation[26]

$$\frac{\mathrm{d}^2V}{\mathrm{d}z^2} = -\frac{e}{\varepsilon_b\varepsilon_0}[N_D^+ - N_A^- - n(z) + p(z)], \tag{1}$$

where ε_b is the static dielectric constant, N_D^+ (N_A^-) is the bulk donor (acceptor) density, assumed constant throughout the sample, and $n(z)$ [$p(z)$] is the electron (hole) density. Equation (1) was solved numerically within the modified Thomas-Fermi approximation (MTFA) following the method described by Veal *et al.*[10] The MTFA correction has been shown[27] to yield profiles that are in good agreement with those obtained from full self-consistent Poisson-Schrödinger calculations. In our calculations, the nonparabolicity of the conduction band[28] is included via the α approximation of the $\mathbf{k}\cdot\mathbf{p}$ interaction and the effects of the potential barrier at the surface are included by the MTFA correction. The InN and GaN parameters used in the simulations are summarized in Table II. The hole parameters of InN have not been well characterized; the theoretical results of Fritsch *et al.*[31] are therefore utilized in these simulations. The calculations are performed assuming a room-temperature value of 300 K, consistent with the experimental measurements. The variation of band gap with composition for the InGaN alloys is described by a bowing parameter of $b=1.4$ eV.[16] Following the empirical relationship $m_e^* \sim 0.07E_g$, the variation of band-edge electron effective mass is assumed to be described by a bowing parameter $b_m=0.07b$. All other quantities are interpolated assuming linear variation with composition.

The resulting CBM, VBM, and carrier concentration profiles for $In_{0.15}Ga_{0.85}N$ are shown in Fig. 4. The bulk hole density of 8.2×10^{17} cm^{-3} was determined by single-field Hall-effect measurements, and so does not account for variations in carrier concentration due to surface or interface effects; it should therefore be taken as an approximate value. This carrier concentration gives a bulk Fermi level approximately 133 meV above the VBM. In contrast, XPS measurements indicate that the surface Fermi level for this sample is pinned approximately 929 meV above the VBM, requiring a downward band bending of 796 meV at the surface, as indicated in Fig. 4(a). This downward band bending increases the separation between the valence band and the Fermi level close to the surface, resulting in the depletion of holes, as shown in Fig. 4(b).

As the In fraction, x, is increased, the surface Fermi level moves further up into the band gap (Fig. 3), resulting in further decrease in near-surface hole density. Once the surface Fermi level is above midgap, electrons accumulate at

TABLE II. The zero-temperature effective mass (in units of the free-electron mass, m_0), spin-orbit (Δ_{so}) and crystal field (Δ_{cr}) splittings, zero-temperature band gap, and Varshni (α and β) parameters of InN and GaN used in the Poisson-MTFA simulations.

	m_e^*	m_{hh}^*	m_{lh}^*	m_{ch}^*	Δ_{so} (meV)	Δ_{cr} (meV)	$E_g(T=0\ \mathrm{K})$ (eV)	α (meV/K)	β (K)
InN	0.048[a]	2.631[b]	2.631[b]	0.080[b]	5[c]	40[c]	0.69[d]	0.41[d]	454[d]
GaN	0.20[c]	1.887[c]	1.887[c]	0.139[c]	17[c]	10[c]	3.51[c]	0.909[c]	830[c]

[a]Based on the empirical relationship $m_e^* \sim 0.07E_g$ (Ref. 29), which is very close to the value of $0.047m_0$ determined by Hofmann *et al.* (Ref. 30) from infrared magneto-optic generalized ellipsometry.
[b]From Fritsch *et al.* (Ref. 31).
[c]From Vurgaftman and Meyer (Ref. 32).
[d]From Wu *et al.* (Ref. 4).

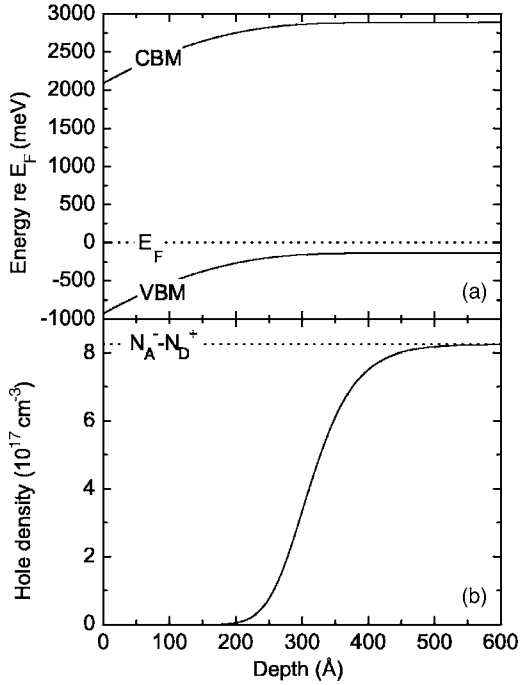

FIG. 4. (a) The position, as a function of depth, of the CBM and VBM (solid lines) relative to the Fermi level (dotted line) for $In_{0.15}Ga_{0.85}N$ calculated by solving the Poisson equation within the MTFA assuming a downward band bending at the surface of 796 meV determined from XPS. The downward band bending leads to a depletion of holes at the surface as shown in (b). The bulk hole density of 8.2×10^{17} cm^{-3} (determined by Hall measurements) gives a bulk Fermi level approximately 133 meV above the VBM.

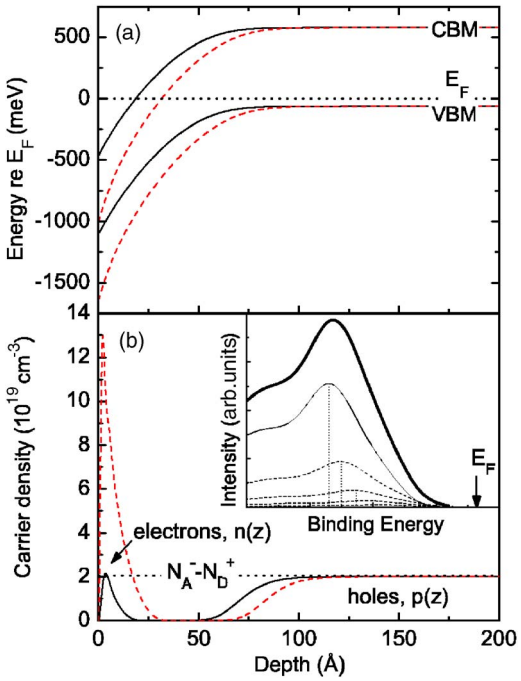

FIG. 5. (Color online) (a) The position, as a function of depth, of the CBM and VBM relative to the Fermi level for InN calculated by solving the Poisson equation within the MTFA assuming a downward band bending at the surface of 1060 meV (solid line) determined from XPS and 1640 meV (dashed line) consistent with universal pinning of the surface Fermi level. The downward band bending is severe, resulting in the Fermi level lying above the CBM at the surface. This causes an inversion layer where electrons are the dominant carrier type at the surface, separated from the bulk hole region by a depletion layer as shown in (b). The bulk hole density of 2×10^{19} cm^{-3} [estimated from the CV profiling of Jones *et al.* (Ref. 9)] gives a bulk Fermi level approximately 60 meV above the VBM. The more severe band bending leads to a larger degree of electron accumulation in the inversion layer at the surface and a wider space-charge region. The inset displays a schematic representation of the underestimation of the VBM to surface Fermi-level separation by XPS measurements in the presence of downward band bending. The total XPS VB emission (bold solid line) is the sum of emission from photoelectrons ejected from the surface (thin solid line) and from photoelectrons ejected from below the surface (thin dashed lines), which have lower intensity (due to the exponential attenuation length of photoelectrons) and smaller VBM to Fermi-level separation than at the surface (due to the downward band bending). The total emission underestimates the VBM to Fermi-level separation compared to the emission from the surface.

the surface. Therefore a *n*-type surface region (inversion layer) exists, which is separated from the *p*-type bulk region by a depletion layer. From Fig. 3, this transition is estimated to occur at an alloy fraction of $x=0.49$ when the effects of the mid-composition sample on the polynomial fit are neglected (due to the lower quality of this sample). Including this sample increases the value of the transition slightly to $x=0.56$.

Poisson-MTFA calculations of the inversion layer formed at the surface of InN are shown in Fig. 5. Due to this inversion layer, electrical properties of the bulk (such as hole concentration) are obscured by the surface *n*-type conductivity and cannot therefore be measured directly by methods such as single-field Hall effect. Recently, Jones *et al.*[9] used electrolyte-based capacitance-voltage (*C-V*) measurements to investigate the space-charge region of the same Mg-doped sample (GS1810) used in this work. A value of the ionized acceptor concentration of 2×10^{19} cm^{-3} estimated from their work is used here, which locates the bulk Fermi level approximately 60 meV above the VBM. If the surface Fermi level is assumed to be pinned at 1120 meV above the VBM (as determined by XPS), this results in a downward band bending of 1060 meV shown (solid lines) in Fig. 5(a), causing the Fermi level to lie well above the CBM at the surface; correspondingly, a surface layer of electrons (an inversion layer) is seen [Fig. 5(b)].

V. DISCUSSION

The space-charge profiles represented here are consistent with the theory of virtual gap states (ViGS),[26] whereby evanescent surface states with complex wave vectors (whose wavefunctions decay exponentially into the vacuum) can exist in the forbidden gap region. ViGS can be induced by, for example, adatoms on the surface or by dangling bonds specific to a given surface reconstruction.[26] These surface states derive from the bulk band structure, and so their character changes from predominantly donor character close to the valence band to predominantly acceptor character close to the

conduction band. The position where they have equal donor- and acceptorlike character is the branch-point energy, E_B. In addition, the states are highly localized, and so their character is determined from contributions from a large proportion of the Brillouin zone and not just the Γ point. Consequently, for InN, where the Γ-point CBM is very low,[33] E_B lies well above the CBM.

Across the composition range, as seen in Fig. 3, the surface Fermi level lies below the branch-point energy for the Mg-doped alloys. Therefore, donor ViGS close to E_B are unoccupied and hence positively charged. For the Ga-rich alloys, this leads to a reduction in the near-surface hole density and hence the depletion layers seen—the positively charged donor surface states are compensated by the background negatively charged acceptors in the hole depletion region. For the In-rich alloys, however, E_B is above the CBM, allowing the ViGS to donate electrons directly into the conduction band, leading to the large accumulation of electrons seen in the inversion layer at the surface. In this analysis, the oxide at the surface has been neglected. In reality, charge transfer will occur between the semiconductor and the more electronegative oxide, influencing the exact pinning position of the Fermi level. The above conclusions, however, hold in general.

It should be noted that the band bending is both more extreme and occurs over a much shorter distance in InN than in $In_{0.15}Ga_{0.85}N$. This has significant consequences for the XPS measurements. The surface specificity of XPS arises due to the attenuation length of the photoelectrons within the solid, with the intensity of detected photoelectrons displaying an exponential decrease with the depth below the surface from which they originate, governed by the Beer-Lambert law. Approximately, 95% of the photoelectron flux can be taken to be generated within the first ~3λ of the surface, where λ is the mean-free path of the photoelectrons, with the largest contribution occurring closest to the surface. However, when there is band bending, as seen here, photoelectrons generated at different depths are associated with different VBM to Fermi-level separations. Neglecting any effects due to surface reconstructions or oxide contamination, the valence-band density of states (VB-DOS) measured by XPS can be seen as the convolution of the bulk VB-DOS with a train of (exponentially reducing in intensity) deltalike functions representing the energy shift with depth of the emitted photoelectrons. In the presence of downward band bending, this acts to broaden the tail of the measured VB spectrum, and hence, the surface VBM to Fermi level separation is underestimated. This is represented schematically in the inset of Fig. 5(b).

From Fig. 3 and a consideration of the relative bulk Fermi levels for *n*-type (close to or above the CBM) and *p*-type (close to the VBM) InN, it can be seen that the band bending is more extreme for Mg-doped than for undoped InN, and so the underestimation of the VBM to Fermi-level separation by XPS will be more severe for the Mg-doped case. Considering this in relation to Fig. 3 suggests that, in reality, the surface Fermi level may be pinned at the same place in both the Mg-doped and undoped InN. In both cases, the bands bend downwards at the surface, requiring donor-type surface states to maintain charge neutrality. It has been shown by

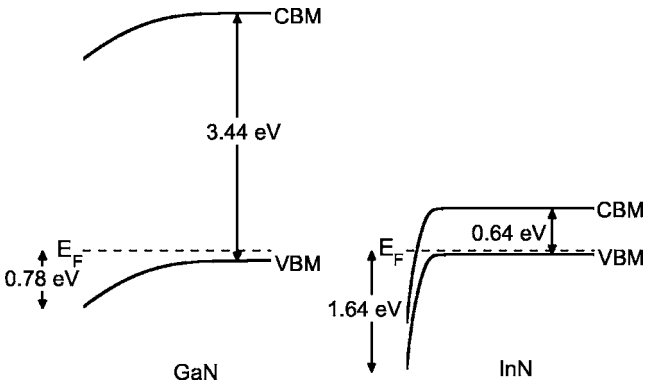

FIG. 6. A schematic representation of the space-charge region in Mg-doped GaN and InN showing the downward band bending present in each case.

Smit *et al.*[34] that for the analogous case of InAs, where the branch-point energy is also located above the Γ-point CBM, exposure to oxygen pins the Fermi level in the same place at the surface independent of the bulk doping. If the surface Fermi level in InN is therefore assumed to be pinned at 1.64 eV above the VBM, as measured by Mahboob *et al.* for *n*-type InN by high-resolution electron energy-loss spectroscopy,[6] the corresponding band bending and carrier-concentration profiles are shown (dashed lines) in Fig. 5. The distance 3λ (the approximate maximum escape depth beneath the surface) is, for the photoelectrons of interest, of the order of 100 Å.[35] This distance covers a sufficient depth (and hence a sufficient portion of the space-charge region and corresponding band bending) to qualitatively justify the XPS measured value of VBM to Fermi-level separation at the surface of ~1.1 eV if the actual value is ~1.6 eV. When the greater degree of downward band bending is considered, a wider space-charge region is formed with a greater degree of electron accumulation in the inversion layer at the surface, consistent with more ViGS able to donate their electrons into the conduction band. The *C-V* profile of Jones *et al.*[9] is very similar to the resulting calculated carrier profile, although it has a slightly higher surface electron density. This could be due to charge transfer associated with the relatively electropositive electrolyte in contact with the InN surface for the *C-V* profiling.

The difference in band bending for Mg-doped GaN and InN samples is summarized schematically in Fig. 6. The InN clearly has a greater degree of, and more rapid, band bending than the GaN. It should be noted that the band bending is downward in both cases. When the Fermi level at the surface is above midgap, an inversion layer results. On the other hand, when the surface Fermi level is below midgap, hole depletion results.

The observed difference in VBM to Fermi-level separation measured by XPS for the undoped and Mg-doped samples indicates that the Mg doping has an effect on the bulk properties. This, coupled with the above discussion of the space-charge region, provides evidence for *p*-type bulk InGaN being achieved by Mg doping across the composition range. In addition, the transition of barrier heights shown in Fig. 2 provides additional evidence for *p*-type bulk conduc-

tivity. The predicted barrier height (CBM to Fermi-level separation) of 2.7 eV for GaN is in good agreement with the value of 2.3 eV measured by Tracy *et al.*[7] for *p*-type GaN when the underestimation of the VBM to Fermi-level separation determined by XPS (discussed above) compared to the more surface sensitive technique of UV-photoelectron spectroscopy employed by Tracy *et al.*[7] is taken into account. A continuous transition of barrier heights is seen across the composition range. The rapid divergence of the barrier heights from those for *n*-type alloys, even for only small Ga fractions, rules out a transition from *n*-type (for In-rich) to *p*-type (for Ga-rich) alloys. This provides further evidence of *p*-type bulk conductivity across the composition range.

VI. CONCLUSION

We have shown that, for Mg-doped $In_xGa_{1-x}N$, a transition from inversion (with an *n*-type surface accumulation layer separated from the *p*-type bulk by a hole depletion layer) for In-rich samples to hole depletion for Ga-rich samples occurs at $x \approx 0.49$. The form of these space-charge regions is consistent with the Mg-doped samples being *p*-type in the bulk across the composition range, and the variation of surface carrier concentration was explained within the concept of virtual gap states. The identification of the *p*-type bulk across the composition range was also confirmed by the difference in barrier heights of the Mg-doped samples compared to undoped samples. Finally, the difference in the XPS measured VBM to Fermi-level separation for the undoped and Mg-doped InN was shown to be consistent with the surface Fermi level being pinned in the same place in both samples, but with the greater degree of band bending for the Mg-doped case causing the XPS measurement to underestimate the true value by more than that for the undoped case.

ACKNOWLEDGMENTS

We are grateful to Danny Law and Graham Beamson of NCESS for their assistance with XPS measurements. Also, we acknowledge the Engineering and Physical Sciences Research Council, UK, for support under Grant No. EP/C535553/1 and for access to the NCESS facility under Grant No. GR/S14252/01.

*Electronic address: c.f.mcconville@warwick.ac.uk
†Permanent address: Department of Physics, Nanjing University, Nanjing 210093, China.

[1] B. Monemar, P. Paskov, and A. Kasic, Superlattices Microstruct. **38**, 38 (2005).
[2] W. Walukiewicz, J. W. Ager III, K. M. Yu, Z. Liliental-Weber, J. Wu, S. X. Li, R. E. Jones, and J. D. Denlinger, J. Phys. D **39**, R83 (2006).
[3] J. Wu, W. Walukiewicz, K. M. Yu, J. W. Ager III, E. E. Haller, H. Lu, W. J. Schaff, Y. Saito, and Y. Nanishi, Appl. Phys. Lett. **80**, 3967 (2002).
[4] J. Wu, W. Walukiewicz, W. Shan, K. M. Yu, J. W. Ager III, S. X. Li, E. E. Haller, H. Lu, and W. J. Schaff, J. Appl. Phys. **94**, 4457 (2003).
[5] J. Wu, W. Walukiewicz, K. M. Yu, W. Shan, J. W. Ager III, E. E. Haller, H. Lu, W. J. Schaff, W. K. Metzger, and S. Kurtz, J. Appl. Phys. **94**, 6477 (2003).
[6] I. Mahboob, T. D. Veal, C. F. McConville, H. Lu, and W. J. Schaff, Phys. Rev. Lett. **92**, 036804 (2004).
[7] K. M. Tracy, W. J. Mecouch, R. F. Davis, and R. J. Nemanich, J. Appl. Phys. **94**, 3163 (2003).
[8] T. D. Veal, P. H. Jefferson, L. F. J. Piper, C. F. McConville, T. B. Joyce, P. R. Chalker, L. Considine, H. Lu, and W. J. Schaff, Appl. Phys. Lett. **89**, 202110 (2006).
[9] R. E. Jones, K. M. Yu, S. X. Li, W. Walukiewicz, J. W. Ager III, E. E. Haller, H. Lu, and W. J. Schaff, Phys. Rev. Lett. **96**, 125505 (2006).
[10] T. D. Veal, L. F. J. Piper, W. J. Schaff, and C. F. McConville, J. Cryst. Growth **288**, 268 (2006).
[11] P. A. Anderson, C. H. Swartz, D. Carder, R. J. Reeves, S. M. Durbin, S. Chandril, and T. H. Myers, Appl. Phys. Lett. **89**, 184104 (2006).
[12] H. Lu, W. J. Schaff, L. F. Eastman, J. Wu, W. Walukiewicz, D. C. Look, and R. J. Molnar, Mater. Res. Soc. Symp. Proc. **743**, 317 (2003).
[13] S. A. Chambers, T. Droubay, T. C. Kaspar, and M. Gutowski, J. Vac. Sci. Technol. B **22**, 2205 (2004).
[14] S. Krischok, V. Yanev, O. Balykov, M. Himmerlich, J. A. Schaefer, R. Kosiba, G. Ecke, I. Cimalla, V. Cimalla, O. Ambacher, H. Lu, W. J. Schaff, and L. F. Eastman, Surf. Sci. **566-568**, 849 (2004).
[15] L. F. J. Piper, T. D. Veal, M. Walker, I. Mahboob, C. F. McConville, H. Lu, and W. J. Schaff, J. Vac. Sci. Technol. A **23**, 617 (2005).
[16] J. Wu, W. Walukiewicz, K. M. Yu, J. W. Ager III, E. E. Haller, H. Lu, and W. J. Schaff, Appl. Phys. Lett. **80**, 4741 (2002).
[17] R. Singh, D. Doppalapudi, T. D. Moustakas, and L. T. Romano, Appl. Phys. Lett. **70**, 1089 (1997).
[18] M. Rao, D. Kim, and S. Mahajan, Appl. Phys. Lett. **85**, 1961 (2004).
[19] J. Zheng and J. Kang, Mater. Sci. Semicond. Process. **9**, 341 (2006).
[20] Z. Liliental-Weber, D. N. Zakharov, K. M. Yu, J. W. Ager III, W. Walukiewicz, E. E. Haller, H. Lu, and W. J. Schaff, J. Electron Microsc. **54**, 243 (2005).
[21] W. Mönch, J. Appl. Phys. **80**, 5076 (1996).
[22] H. Lüth, Phys. Status Solidi A **187**, 33 (2001).
[23] T. U. Kampen and W. Mönch, Appl. Surf. Sci. **117-118**, 388 (1997).
[24] S. X. Li, K. M. Yu, J. Wu, R. E. Jones, W. Walukiewicz, J. W. Ager III, W. Shan, E. E. Haller, H. Lu, and W. J. Schaff, Physica B **376**, 432 (2006).
[25] J. Robertson and B. Falabretti, J. Appl. Phys. **100**, 014111 (2006).
[26] W. Mönch, *Semiconductor Surfaces and Interfaces* (Springer, Berlin, 2001).
[27] G. Paasch and H. Ubensee, Phys. Status Solidi B **113**, 165

(1982).
[28] J. Wu, W. Walukiewicz, W. Shan, K. M. Yu, J. W. Ager III, E. E. Haller, H. Lu, and W. J. Schaff, Phys. Rev. B **66**, 201403(R) (2002).
[29] B. R. Nag, Phys. Status Solidi B **237**, R1 (2003).
[30] T. Hofmann, T. Chavdarov, V. Darakchieva, H. Lu, W. J. Schaff, and M. Schubert, Phys. Status Solidi C **3**, 1854 (2006).
[31] D. Fritsch, H. Schmidt, and M. Grundmann, Phys. Rev. B **69**, 165204 (2004).
[32] I. Vurgaftman and J. R. Meyer, J. Appl. Phys. **94**, 3675 (2003).
[33] I. Mahboob, T. D. Veal, L. F. J. Piper, C. F. McConville, H. Lu, W. J. Schaff, J. Furthmüller, and F. Bechstedt, Phys. Rev. B **69**, 201307(R) (2004).
[34] K. Smit, L. Koenders, and W. Mönch, J. Vac. Sci. Technol. B **7**, 888 (1989).
[35] D. P. Woodruff and T. A. Delchar, *Modern Techniques of Surface Science*, 2nd ed. (Cambridge University Press, Cambridge, 1994).